Optimal Transmission Range and Charging Time for Qi-Compliant Systems

Alexander D. de Sousa, Luiz F. M. Vieira, *Member, IEEE*, and Marcos A. M. Vieira, *Member, IEEE*

***Abstract*—Although widespread in the market, the wireless power transfer devices following the Qi Standard suffer from limited transmission range and link instability. Previous works often address these issues by proposing improvements for both transmitting and receiving sides, which disposes of the Qi interoperability and ease of purchasing. This article proposes an optimal transmitting-range-maximization algorithm for the receiving part of a Qi-compliant system. The algorithm actuates over the receiving circuit by dynamically adjusting its internal impedance. The proposed method obtains the optimal result in $\Theta(1)$ time and does not require any direct information from the transmitting part neither any preparameterized data. Simulation results indicate that the proposed algorithm can mitigate the issue of re-establishing the link when the coils are loosely coupled.**

***Index Terms*—Inductive coupling, inductive power transfer, optimization, Qi, wireless charging vehicle, wireless networks, wireless power transfer (WPT).**

I. Introduction

THE wireless power transfer (WPT) is a widespread and still growing technology in the market. According to a report by *MarketsandMarkets* research firm, the wireless-power-transmission market is expected to reach $17.04 billion by 2020 [1]. There are already some standards defined for WPT, in particular regarding mobile and low-power devices. Among these, the *Qi Standard* [2], defined by the *Wireless Power Consortium* (WPC) for *inductive power transfer* (IPT), is one of the most popular. In particular, Qi-certified devices and chargers grew about 77% in 2018 with global volumes, exceeding 366 million devices around the world [3]. However, despite being cheap and affordable, Qi-compliant devices reach quite small transmission ranges and, therefore, they are not commonly employed to most WPT applications, such as *automated charging* [4] [5] of *low-power wireless networks*.

The Qi-certified devices are usually designed to prioritize high efficiency at a few millimeters instead of allowing higher transmitting ranges. Simply improving the transmitting range of a Qi device is not a difficult task, but doing it while maintaining complete Qi-compliance is quite harder. Indeed, the main advantages of Qi are the interoperability and ease of access, since one may implement a Qi-based WPT system using only off-the-shelf devices. To take advantage of the referred interoperability, at least one of the sides of the transmitting system must be completely preserved and, thus, be implemented using ready-to-use commercial devices. Improving the power transmission side is relatively simple, since the simple enlargement of the maximum allowed power consumption, coil size, or number of turns of the coil leads to range enhancement of IPT systems [6], the employment of multiple-input-multiple-output (MIMO) transmitting setups enables reaching larger distances [7] and the poor resilience of the data connection (see Section V) can be mitigated by making the power transmitter policies more tolerant to packet losses. Improving the receiving side, in turn, is more challenging, since the data transmission in Qi occurs exclusively from the power receiver to the power transmitter and, therefore, the receiver does not have explicit information toward the transmitter. Furthermore, there is a large variety of Qi-certified power transmitters, so preparameterization is not always feasible.

The main contribution of this article is the proposition of an optimal transmitting-range-maximization algorithm for the receiving part of a Qi-compliant system. The algorithm only requires the transmitting part to be Qi-compliant and actuates over the receiving circuit by dynamically adjusting its internal impedance. This is a completely novel idea since other literature work either requires modifications toward the transmitting part or admit circuit models different than the typical ones used by Qi systems (see Section II). Although the associated optimization problem involves *quadratic fractional programming* [8], whose general case is *NP-hard*, our solution is entirely based on analytical closed formulas and, therefore, its execution is very efficient and compatible with the context of the embedded systems. The other advantages of the proposed algorithm are summarized as follows.

1) It either responds the optimal solution or indicates the algorithm cannot provide it.
2) The electrical parameters of the system are not required to be explicitly acquired. Instead, the algorithm performs the optimization process using only two scalar parameters acquired from the receiving current measurements.
3) The parameter acquisition requires storing only the last three measurements of impedance and current and, therefore, it requires asymptotically constant memory space.

Manuscript received January 23, 2020; revised April 3, 2020; accepted May 14, 2020. Date of publication May 24, 2020; date of current version July 31, 2020. This work was supported in part by the Coordenação de Aperfeiçoamento de Pessoal de Nível Superior—Brasil (CAPES)—Finance Code 001, in part by the Conselho Nacional de Desenvolvimento Científico e Tecnológico (CNPq), and in part by the Fundação de Amparo á Pesquisa do Estado de Minas Gerais (FAPEMIG). Recommended for publication by Associate Editor J. Acero. *(Corresponding author: Alexander D. de Sousa.)*

The authors are with the Computer Science Department, Universidade Federal de Minas Gerais, Belo Horizonte 31270-901, Brazil (e-mail: alexanderdecker@dcc.ufmg.br; lfvieira@dcc.ufmg.br; mmvieira@dcc.ufmg.br).

Color versions of one or more of the figures in this article are available online at https://ieeexplore.ieee.org.

Digital Object Identifier 10.1109/TPEL.2020.2996999

4) There are no requirements for the transmitting part besides being Qi-compliant, including fixed parameters and impedance adjustment/matching policies.
5) The instability and low resilience for loosely coupling situations are naturally mitigated.

We explore the employment of Qi to the automated charging of wireless sensor networks (WSNs) as a study case to motivate the improvement of the transmitting range. We identify the instability and low resilience of the communication link as one of the most notable issues when the power transmission is performed while the coils are loosely coupled. Besides keeping the transmitting side untouched and unrestricted but being Qi-compliant, we differ from other literature works as we base our modeling on a 4-port network, which is consistent with the design of general Qi devices. Indeed, both transmitting and receiving coils are bifilar, which means each one is equivalent to a pair of high coupled parallel coils.

II. Related Work

This section summarizes the literature work related to the automated charging of low-power wireless nodes, which is the main use case of this work, and related to general improvements of Qi Standard. Many works have been developed addressing the automated recharging of wireless sensor nodes, especially for the terrestrial environment. The employed methods are many, but it is notable that the vast majority avoids using inductive coupling methods, due to their typical low range. Indeed, most works prefer using less efficient methods but those reach longer distances, such as far-field transmission. Zuquim *et al.* [9] propose an extended power state machine to ensure low power consumption. In the work by Bhatti *et al.* [10], laser beams of 0.8 W are used for recharging wireless nodes. Although energetically efficient, it is highly dependent on alignment and line of sight. In the work by Peng *et al.* [4], the radio-frequency-based standard defined by *PowerCast* [11] is embedded in a robot, which travels through the network in order to recharge the nodes that requested its service.

The inductive coupling is addressed by Xie *et al.* [5], which propose a nonlinear optimization problem related to the scheduling of the nodes recharging, thus abstracting several low-level aspects of the system. So, despite considering the same case of use as this article, they address a different problem regarding automated recharging. Other works already proposed modifications for parts of the IPT setup while aiming for the maintenance of Qi-compliance. Hwang *et al.* [12] propose an integrated circuit that can be used with Qi, PMA, or A4WP transmitters. These standards vary significantly regarding the used frequency range, and therefore, a set of frequency-optimized independent coils was used instead of a single one. Berger *et al.* [13], in turn, propose an integrated circuit that implements the receiver-side Qi protocol, evaluating three modes of current rectification—a passive, a semiactive, and a fully active fashion. Finally, Solar *et al.* [14] test a novel geometry for the receiving coil, which aims for minimizing the size of the receiving device.

As far as we know, no work in the literature has specifically sought to optimize the impedance of the receiving part of a Qi-compliant system, regardless of the transmitting part. When there is no guarantee of cooperation of the transmitting part, the widespread method of impedance matching [15] is not always applicable, since the receiver cannot indiscriminately decrease its own resistance in the case where the impedance of the transmitter is less resistive. Furthermore, the literature works usually address other WPT setups rather than usual Qi ones (see Section III), such as simple *RLC* rings for the transmitter and receiver parts [16], [17] and simple *RLC* rings with intermediate resonators for wave guiding [15], [18]. Thus, the utilization of a model that addresses the *bifilar* characteristic of the Qi coils also represents a contribution to the state of the art.

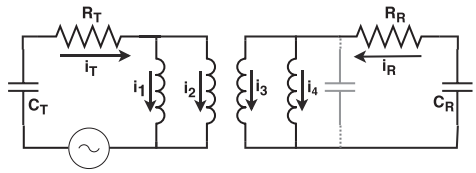

Fig. 1. Scheme of the simplified circuit used for the modeling.

III. Modeling

Both transmitting and receiving coils have two parallel filaments when following the Qi specification. The two coupled circuits that form a Qi system can be simplified as in the scheme from Fig. 1. Apart from the two-filament coil, the transmitting part is an active *RC* circuit. The receiving part, in turn, has also a parallel capacitor. Nonetheless, the capacitance value of the component represented in gray is quite small when compared with the other capacitors, so it is omitted from our modeling for simplification purposes. Indeed, the assumed modeling is the same as the one applied for the simulations from Section V, reaching good accuracy by just faintly adjusting the value of the series capacitor. In the stationary state, the set composed of the powered device and the battery charger is modeled as a resistor, while the square wave signal used in Qi transmitters is approached to a sinusoidal wave [19]. Thus, by applying the *Kirchhoff Voltage Law*, the four equations listed ahead are obtained. v is the phasor-notation voltage of the source, w is the operating angular frequency of the signal, and M is the matrix in which $M_{n,k}$ is the mutual induction between the nth filament and the kth one. For simplification purposes, $M_{n,n}$ is the opposite of the self-inductance of the nth filament for all n

$$\begin{cases} v = R_T i_T - \frac{\sqrt{-1}}{wC_T} i_T - \sqrt{-1} w \left(\sum_{k=1}^{4} M_{1,k} i_k \right) \\ v = R_T i_T - \frac{\sqrt{-1}}{wC_T} i_T - \sqrt{-1} w \left(\sum_{k=1}^{4} M_{2,k} i_k \right) \\ 0 = R_R i_R - \frac{\sqrt{-1}}{wC_R} i_R - \sqrt{-1} w \left(\sum_{k=1}^{4} M_{3,k} i_k \right) \\ 0 = R_R i_R - \frac{\sqrt{-1}}{wC_R} i_R - \sqrt{-1} w \left(\sum_{k=1}^{4} M_{4,k} i_k \right) \end{cases} . \tag{1}$$

The methods described in this section are based on adjusting the impedance of the receiving part, without considering the inductive reactance. Thus, it is useful to define $Z_R + \Delta Z_R \triangleq R_R - \frac{\sqrt{-1}}{wC_R}$, where Z_R is the fixed impedance of the circuit (resistance and capacitive reactance) and ΔZ_R is the variable

one. It is also useful to define $\vec{u}_1 \triangleq [1,1,0,0]^t$, $\vec{u}_2 \triangleq [0,0,1,1]^t$ and

$$Z \triangleq -\sqrt{-1}wM + \left(R_T - \frac{\sqrt{-1}}{wC_T}\right)\vec{u}_1\vec{u}_1^t + Z_R\vec{u}_2\vec{u}_2^t.$$

By applying the *Kirchhoff Current Law*, we find $i_T = i_1 + i_2$ and $i_R = i_3 + i_4$. Substituting it in (1), it follows that

$$v\vec{u}_1 = (Z + \Delta Z_R\vec{u}_2\vec{u}_2^t)\vec{i}.$$

Assuming $det(Z + \Delta Z_R\vec{u}_2\vec{u}_2^t) \neq 0$, the electric current vector can be obtained using

$$\vec{i} = v(Z + \Delta Z_R\vec{u}_2\vec{u}_2^t)^{-1}\vec{u}_1. \tag{2}$$

As ΔZ_R is a scalar, the *Sherman–Morrison* formula [20, p. 65] can be applied to (2) for obtaining

$$\vec{i} = vZ^{-1}\vec{u}_1 - \frac{\Delta Z_R}{1 + \Delta Z_R\vec{u}_2^tZ^{-1}\vec{u}_2)}vZ^{-1}\vec{u}_2\vec{u}_2^tZ^{-1}\vec{u}_1 \tag{3}$$

For the sake of clarity, let us make some more definitions. Let a and b be defined as

$$a \triangleq \vec{u}_2^tZ^{-1}\vec{u}_2 \quad b \triangleq v\vec{u}_2^tZ^{-1}\vec{u}_1.$$

As $i_R = \vec{u}_2^t\vec{i}$, it follows that

$$i_R = b - \frac{ab \cdot \Delta Z_R}{1 + a \cdot \Delta Z_R}. \tag{4}$$

1) Optimization Problem: We choose the receiving resistance and capacitance as decision variables because of the ease of controlling these parameters. We assume the receiver has a digital potentiometer in series with the stationary resistor and a digital varicap in parallel with the capacitor. The objective of the optimization algorithm is to maximize the dc current that charges the battery. Assuming the conversion efficiency increases monotonically as the input current increases, we can simplify the objective function by redefining it as maximizing the *Euclidean norm* of the receiving current i_R, which means $Z_R^* = \arg\max\{\sqrt{i_R\bar{i}_R}\}$. Furthermore, maximizing purely $i_R\bar{i}_R$ is also an equivalent objective function. The values of Z_R acceptable as feasible must be restricted in order to guarantee at least the resistance is always positive and the capacitive reactance is ever negative. We consider a further restriction to guarantee the resistance has a lower bound equal to the equivalent resistance of the set composed by the current converter, the battery charger, and the powered device. Analogously, the capacitance value is also limited by the fixed capacitor. So, the optimization problem can be stated as in

$$\begin{aligned} \Delta Z_R^* = \arg\max\ & \{i_R\bar{i}_R\} \\ \text{s.t.}\quad & \mathrm{Re}(\Delta Z_R) > 0 \\ & \mathrm{Im}(\Delta Z_R) < 0. \end{aligned} \tag{5}$$

Using (4) and assuming $1 + a \cdot Z_R \neq 0$—which is pretty reasonable, since it would imply on infinity electrical current, the objective function can be rewritten as

$$\arg\max\ \left\{\left(-\tfrac{ab\cdot\Delta Z_R}{1+a\cdot\Delta Z_R} + b\right)\left(-\tfrac{\bar{a}\bar{b}\cdot\Delta \bar{Z}_R}{1+\bar{a}\cdot\Delta \bar{Z}_R} + \bar{b}\right)\right\}.$$

Expanding the terms, we obtain the following equation. Notice that the term $|b|^2$ is constant toward Z_R, and therefore, it can be disregarded

$$\arg\max\ \left\{\left(\tfrac{ab\cdot\Delta Z_R}{1+a\cdot\Delta Z_R}\right)\left(\tfrac{\bar{a}\bar{b}\cdot\Delta \bar{Z}_R}{1+\bar{a}\cdot\Delta \bar{Z}_R}\right) - 2\mathrm{Re}\left(\tfrac{a|b|^2\Delta Z_R}{1+a\cdot\Delta Z_R}\right)\right\}.$$

After algebraic manipulations, the following is obtained:

$$\arg\max\ \left\{\tfrac{-|b|^2|a\cdot\Delta Z_R|^2 - 2|b|^2 Re(a\cdot\Delta Z_R)}{|1+a\cdot\Delta Z_R|^2}\right\}.$$

Using the identity $|\theta+1|^2 = |\theta|^2 + 2\mathrm{Re}(\theta) + 1\ \forall\,\theta \in \mathbb{C}$, the expression can be reformulated as follows:

$$\arg\max\ \left\{\tfrac{-|b|^2(|1+a\cdot\Delta Z_R|^2 - 1)}{|1+a\cdot\Delta Z_R|^2}\right\}.$$

Finally, the expression can be simplified by first removing constant addends and then the constant nonnegative factor $|b|^2$, which results in

$$\arg\max\ \left\{\tfrac{1}{|1+a\cdot\Delta Z_R|^2}\right\}. \tag{6}$$

Let us change the decision variables to $x \triangleq \mathrm{Re}(a \cdot \Delta Z_R) + 1$ and $y \triangleq \mathrm{Im}(a \cdot \Delta Z_R)$, in order to deal with a real search space. Notice that the transformation from ΔZ_R to (x, y) is a bijection and the value of ΔZ_R can be recovered using

$$\Delta Z_R = \frac{x - 1 + \sqrt{-1}y}{a} = \frac{(x - 1 + \sqrt{-1}y)\bar{a}}{|a|^2}. \tag{7}$$

Notice that (6) has always nonnegative numerator and denominator, and therefore, it is equivalent to the minimum argument of its inverse. Substituting the new definitions in (6), the expression in the following equation is obtained;

$$\arg\min\ \left\{x^2 + y^2\right\}. \tag{8}$$

The restrictions of the problem can be rewritten using (7) and then be constructed in terms of the $< x, y >$ variables, as shown in

$$\begin{cases} \mathrm{Re}(\Delta Z_R) = \frac{\mathrm{Re}(a)(x-1)+\mathrm{Im}(a)y}{|a|^2} \geq 0 \\ \mathrm{Im}(\Delta Z_R) = \frac{\mathrm{Re}(a)y-\mathrm{Im}(a)(x-1)}{|a|^2} \leq 0 \end{cases}. \tag{9}$$

Lemma III.1: Let the optimization problem whose objective function is defined by (8) and whose feasible area is determined by (9). Assuming the origin of coordinates is outside the feasible area, there is always an optimal solution over the feasibility frontier.

Proof: The optimization problem defined by (8) and (9) is equivalent to finding the closest feasible point P to the origin of the coordinates $\hat{O}$, considering the *Euclidean distance*. Suppose the optimal point P is not over the frontier. So, the frontier divides the xy-plane into two partitions, one containing P and the other containing $\hat{O}$. As the frontier is continuous, the *Intermediate Value Theorem* guarantees that the segment $\overline{PO}$ and the frontier intersect each other. Considering the Euclidean geometry, the intermediate point is less distant from $\hat{O}$ than P and, therefore, P is not optimal, which leads to a contradiction.■

Lemma III.2: Let the problem of finding d^* such that

$$d^* = arg\,min\{x^2 + y^2 | (y = m_1x + m_2) \wedge (sx \geq sx_0)\}$$

where $x, y, m_1, m_2, x_0 \in \mathbb{R}$, and $s \in \{-1, 1\}$. The optimal solution is either (i) $(x = -\frac{m_1 m_2}{m_2^2+1}, y = \frac{m_2}{m_2^2+1})$ or (ii) $(x = x_0, y = m_1 x_0 + m_2)$.

Proof: Substituting $y = m_1 x + m_2$ in $d = x^2 + y^2$, the following is obtained:

$$d = (m_1^2 + 1)x^2 + 2m_1 m_2 x + m_2^2$$

which is a second-degree function whose only critical point is at $x_1 = -\frac{m_1 m_2}{m_2^2+1}$. If this point is such that $sx_1 \geq sx_0$, alternative (i) is trivially satisfied. Otherwise, the point that minimizes d is at x_0, because the second-degree function is monotonic for any continuous interval that does not contain the vertex of the parabola. In case, $(x_0, y = m_1 x_0 + m_2)$ is the closest feasible point to the vertex (considering the *Euclidean distance*), so it is the argument that maximizes d inside the interval $[x_0, s \cdot \infty)$ and, therefore, alternative (ii) is satisfied. ■

Theorem III.3: Assuming $\hat{O}$ is not feasible, the solution of the optimization problem defined by (8) and (9) is either i) the point of the line $Re(\Delta Z_R) = 0$, which is closest to the origin, ii) the point of the line $Im(\Delta Z_R) = 0$, which is closest to the origin, or iii) the intersection point between $Re(\Delta Z_R) = 0$ and $Im(\Delta Z_R) = 0$.

Proof: According to Lemma III.1, the optimal solution of the problem is over the feasibility frontier. So, it is equivalent to

$$\arg\min\{\min\{x^2 + y^2 | x \in F_R\}; \min\{x^2 + y^2 | x \in F_I\}\}$$

where F_R is the feasible interval of $\text{Re}(\Delta Z_R) = 0$ and F_I is the feasible interval of $\text{Im}(\Delta Z_R) = 0$. According to Lemma III.2, the solution of each subproblem is the closest point of each straight line to the origin—in the case that it is feasible—or, alternatively, the point at x_0, which is trivially what we intended to prove. ■

Notice that $\hat{O}$ being inside the feasible area is impractical considering the values of a realistic application. Indeed, the global maximum is the positive-infinite one-sided limit as (x, y) approaches to (0, 0), which would imply an infinite receiving current. So, Theorem III.3 allows finding the optimal solution to the problem asymptotically in constant time and using constant space, but assumes the voltage source is always powerful enough to provide the required active-power. The case where the source eventually gets saturated is addressed in Sections IV and III-A2.

2) Parameter Acquisition: Let $\{{}^k i_R \mid k \in \mathbb{N}\}$ be a list of the electric current vector samples short spaced in time so that the M matrix and w can be considered as constants. In this case, the only nonconstant parameter is ΔZ_R, which is also stored in the form ${}^k\Delta Z_R$, for each generated current ${}^k i_R$. Furthermore, a and b are also constants. Those pairs $\langle {}^k\Delta Z_R, {}^k i_R \rangle$ are related as in (4), and therefore, the resulting equations can be easily linearized as ${}^k\Delta Z_R {}^k i_R a - b = -i_R$, which allows obtaining $\langle a, b \rangle$ parameters using the *minimum squares method*. However, we use here a bit more complex method, which has the advantage of allowing the verification of the obtained parameters. Indeed, the voltage source can eventually get saturated, which may invalid the obtained data. Let ${}^k dI_R \triangleq {}^k i_R - {}^{k-1} i_R$. Subtracting two adjacent current measurements, it follows that

$${}^k dI_R = \frac{({}^{k-1}\Delta Z_R - {}^k\Delta Z_R)ab}{{}^k\Delta Z_R {}^{k-1}\Delta Z_R a^2 + ({}^k\Delta Z_R + {}^{k-1}\Delta Z_R)a + 1}.$$

Algorithm 1: Behavior of the Receiving Part.

```
while ω >110 kHz do
  Ask TX to increase power
end while
loop
  Try inferring the parameters
  if successful then
    Register the previous values of current and impedance
    ΔZ_R ← the optimal impedance
    Decrease σ, limiting it to 0
  else if saturation condition then
    ΔZ_R ← a safe value of impedance
  else
    ΔZ_R ← a safe value of impedance
    Increase σ
  end if
  Apply ΔZ_R + |Z(0; σ)|
  Ask TX to keep the power
end loop
```

Linearizing the equation, we achieve (10), where the matrix form of minimal squares method is already applied:

$$\left[a^2, a, ab\right]^t = -(Q^* Q)^{-1} Q^{*k} dI_R. \tag{10}$$

Here, Q is the coefficient matrix where each line follows the structure as

$${}^k\vec{q} = \begin{bmatrix} {}^k dI_R {}^k\Delta Z_R {}^{k-1}\Delta Z_R \\ {}^k dI_R({}^k\Delta Z_R + {}^{k-1}\Delta Z_R) \\ {}^k\Delta Z_R - {}^{k-1}\Delta Z_R \end{bmatrix}^t.$$

Having a number of rows greater than or equal to 3 is a necessary condition for Q^*Q to be nonsingular, even though such a condition is not sufficient.

The first element of the inferred vector must be close to the square of the second one. Otherwise, 1) the measurement error was too high, 2) the M matrix changed excessively from sample to sample, or 3) the voltage supply was saturated, which means an excessive power was required and consequently its internal resistance increased.

IV. Implementation

The method described in this section is briefly presented in Algorithm 1. It is divided into two phases. The first one aims to force the transmitter to reach as near as possible to the resonance frequency of 100 kHz, that is, for the operating range of Qi, to 110 kHz.

After that, the receiver repeats calculating the best values of impedance, applying the values, updating the collected data, and asking the transmitter (TX) to maintain the power. In the case where the algorithm fails obtaining the parameters, a default receiving-impedance is applied. This "safe" value must be chosen in a way that the saturation condition is avoided. The failure may occur either because: a) Q is singular or b) the value of the first element of the inferred vector is not close enough

TABLE I
MOST NOTABLE PARAMETERS FOR THE SIMULATION OF THE WPT USING QI STANDARD

Parameter	Value
Resistance (TX)	0.015 Ω
Resistance (RX)	3.95 Ω
Capacitance (TX)	400 nF
Capacitance (RX)	100 nF
Maximum Consumed Power	7.5 W
TX coil excitation voltage	5 V
Magnetic Permeability	$1.26{\cdot}10^{-6}\ Hm^{-1}$
Coil Model (TX)	WE-WPCC 760308111
Coil Model (RX)	IWAS-4832FF-50

to the square of the second one. If the alternative (a) is true, the receiver increases the random *Gaussian* (**Z**) addend of the applied resistance, in order to increase the variability between the lines of the Q matrix. Otherwise, there is no alternative but to try to apply a "safe" impedance and wait until the system is stable.

Since the control messages defined by WPC are modulated using two receiving impedance values, the dynamic adjustment affects the communication in a way similar to external noise. So, the updating rate of the impedance must be small enough to guarantee the communication. This algorithm is consistent with Qi as it does not require explicit information from the transmitting part. Since Qi offers no means for obtaining readings from the transmitter, admitting extra information would violate the standard. Moreover, since the Qi transmitter is not required to have impedance adjustment, the algorithm does not admit the existence of such a feature. However, the algorithm naturally adapts to the impedance adjustment of the transmitter if it exists.

V. EXPERIMENTAL RESULTS

WSN are sometimes deployed in difficult access environments, such as deep-sea, which makes it difficult for a human operator to replace the batteries of each device. Some works address this issue via *energy harvesting* [21], which is limited on practice [5], since the success of the technique is highly dependent on the characteristics of the environment. Other works, in turn, use *automated charging*, which allows each device to be smaller, but requires the use of a robot that travels through the network while providing power to the nodes—often using WPT. The employment of WPT-based charging is more cost-effective than wired charging, since it reduces the cost of deployment and maintenance of cables and connectors [22]. This section addresses the employment of Qi Standard to WSN. First, we emulate the automated charging procedure and use receiving voltage measurements to identify issues regarding the regular Qi. We then introduce a test procedure under controlled conditions to facilitate the reproduction of results in a simulated environment and the comparison with the algorithms developed here.

1) Automated Charging: The experiment setup consists of an TI MSP430 device and an iRobot create. Table I shows some parameters considered for the experiments. The MSP430 represents a rechargeable low-power wireless node and the robot is responsible for carrying a battery and the Qi transmitter. This setup is shown in Fig. 2. The powered device keeps constant its

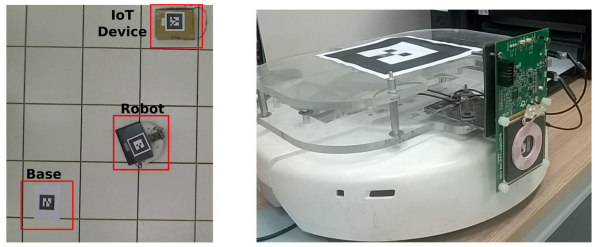

(a) (b)

Fig. 2. Experiment setup and a iRobot create attached to a Qi transmitter.

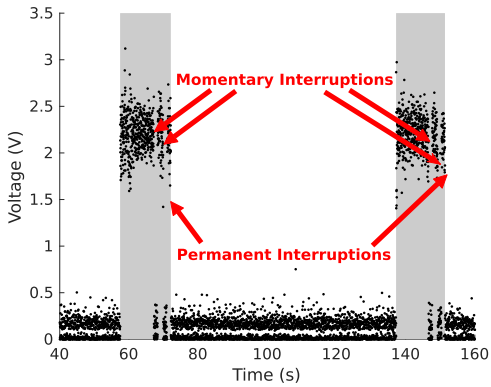

Fig. 3. Brief excerpt from the voltage temporal series obtained from the robot experiment. The gray rectangles represent the time intervals in which the robot attempted to transfer power before having to restart searching for a good placement for the power transmitter.

equivalent resistance so that the variations of transmitted power are mainly due to variations in the coupling factor between the coils.

The charging procedure is defined as follows. The robot is driven from the base to the powered device. There, it waits for a few moments, being able to perform a recharge operation. In the end, it returns to the base. This procedure is then repeated 33 times while the receiving voltage is measured. Fig. 3 shows a brief excerpt from the voltage temporal series obtained from the robot experiment, contemplating two moments in which the robot approaches the MSP430. In order to better analyze the data, we establish a threshold of 1.5 V for considering the measured voltage being from a successful attempt of WPT. We establish a second threshold of 10 s for determining if an eventual disconnection is momentary or permanent. In short, if the voltage drops below 1.5 V for more than 10 s, we consider the WPT attempt to be finished. The gray rectangles in Fig. 3 represent each individual attempt to approach the MSP430. Notice that during the approaches, especially at the end of both, the connection between transmitter and receiver is lost several times. It is re-established a few times but eventually culminates in a longer final disconnect. After the end of each attempt, the robot has no other option than retry posing itself to start a new connection.

Fig. 4 shows the histogram representations of some notable quantities regarding the collected data. These values include the total time in which the WPT effectively occurs in each

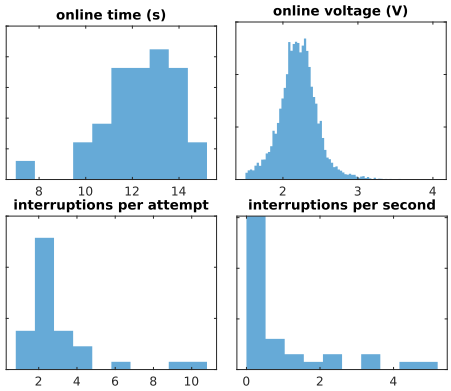

Fig. 4. Histogram representations of some notable quantities obtained from the collected data.

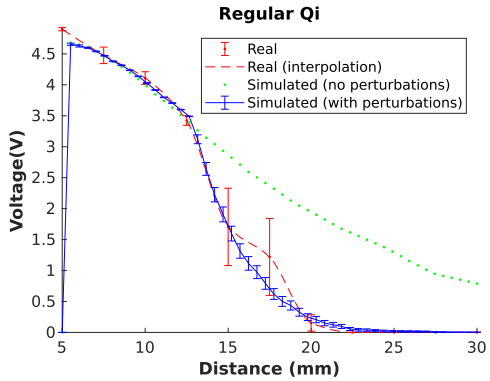

Fig. 5. Comparison between simulated and real-world data.

attempt—*online time*, the number of link interruptions per attempt, the average number of link interruptions per second for each attempt—*link interruption ratio*, and the received voltage without considering the measurements below 1.5 V—*online voltage*.

2) Voltage Decay Experiment: This experiment focuses on studying the decay of the receiving voltage for different distances between transmitter and receiver. So, we keep the coil planes parallel and the centroids aligned, varying only the distance between them. The results are represented by the dashed line from Fig. 5, considering five repetitions. The 95% confidence interval is estimated using Student's-*t* distribution with 4 degrees of freedom. We reproduce the real-world experiment in a simulated environment to better evaluate the issues regarding it and then we use the conclusions for developing improvements. The simulator is the successor of the *WPTSimulator* [23], which is currently available on github.com/AlexDecker/sdWPT-Simulator. The simulations are performed using one active node and one passive node. The active one is composed of an alternate-voltage generator, a voltage sensor, the controller, and an *RLC* circuit. The behavior of the controller is defined according to *Qi 1.0* specification and the network communication is modeled using the *SINR* model, whose threshold $\beta = 0.225$ is obtained via tuning. The parameters regarding the circuit of the transmitting part are obtained from the datasheet of the *bq500212 A* evaluation kit and from the sheets of its components. Finally, the 7.5-W saturation limit for the voltage source is calculated by multiplying the typical input current by the typical input voltage of the *bqTesla* Qi transmitter. The passive one, in turn, is composed of an *RLC* circuit with a bifilar coil, a current converter, a controller whose behavior also follows Qi 1.0 specification, a reactance-based SWIPT transceiver, and a Li-ion battery. Analogously, the parameters of the circuit are obtained from the datasheets of the components of the STEIN WPT-adapter [24]. The equivalent resistance of the set converter/charger/device is obtained by the ratio between the dropped voltage and the receiving current, resulting in 3.97 Ω.

The result is shown in Fig. 5. Notice that the simulated data (dotted line) overlaps the reference line (red dashed line) until about 12.5 mm and, after that, dispel from it more and more. For further analyzes, we disregard the data until 6.125 mm, which is negatively affected by the initialization of the algorithm. So, for the interval 6.125–12.5 mm, the *Pearson Correlation* between the real and the simulated curves is 0.9931, whereas the mean-squared error is 0.0042 V^2, which implies high goodness of fit. After 12.5 mm, in turn, the correlation is 0.8878 and the mean-squared error is 1.6594 V^2. Admitting a probability of 0.27% for each continuing message to be dropped due to perturbations in the medium, the data represented by the continuous line are obtained. For the considered parameters of SINR, the disrupted link can be re-established up to 12.5 mm far. After that, the connection is permanently lost after a single continuing message is dropped and, therefore, the average voltage decreases as the distance increases. Considering the perturbations, the simulated and the real series achieve a correlation of 0.9954 and a mean-squared error of 0.0286 V^2. Indeed, the mode of the observed number of momentary link interruptions for each repetition of the simulated experiment is 2, whereas the mode of the momentary link breaks for each attempt of the robot experiment (see Section V-A1) is also 2.

3) Discussion: According to Fig. 4, most voltage measurements considering the online moments are between 2 and 2.5 V, which indicates that the most common state of the system is loosely coupled. For these situations, the transmitting algorithm converges to 110 kHz. Therefore, as the load resistance is kept constant, the only variable influencing the receiving voltage is the mutual coupling between the coils. From Fig. 5, one can estimate the most common coupling factors in the automated charging experiment as being the same achieved when the coils are aligned and the distance apart the centroids is between 17.5 and 20 mm. Notice that it does not mean the coils in the automated charging experiment were aligned or this distance apart. Instead, it means the coupling between the coils is not enough to allow the re-establishment of connection most times. Indeed, most attempts end after two momentary link interruptions and last for just a few seconds—between 11 and 14 s, which is far from the desired, since the time required to charge most *Li-ion* batteries starting from a dead charge is about 1 h.

4) Simulations of the RX-Improved Algorithm: We maintain the setup and parameters employed in previous simulations (see Section V-A2) to evaluate the impact of using different algorithms for the receiver side. The simplest modification for the receiving side consists of setting the equivalent capacitance to 163.21 μF, in order to make the passive circuit resonate at 4 kHz, that is, the frequency of the analog ping. So, this strategy

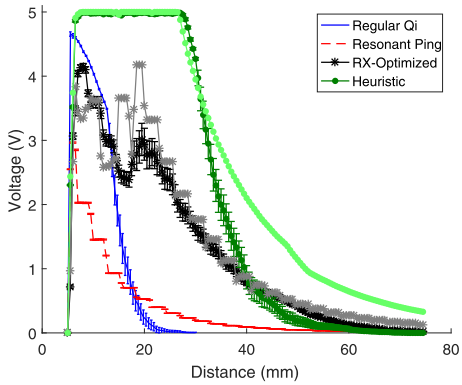

Fig. 6. Decay of the received voltage in relation to the distance between the centroids of the coils. The RX-Improved algorithm and the Omniscient Heuristic simulations consider both with perturbations in the medium (dark shades) and without perturbations (light shades).

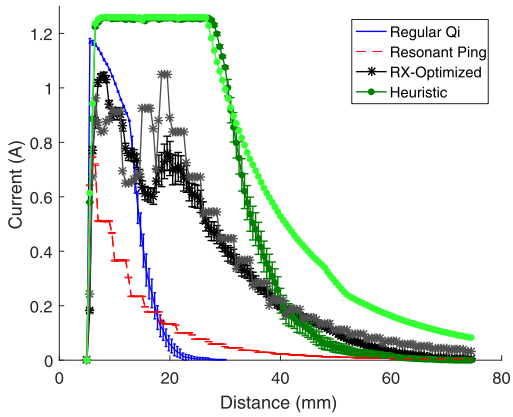

Fig. 7. Decay of the received rectified current in relation to the distance between the centroids of the coils. The RX-Improved algorithm and the Omniscient Heuristic simulations consider both with perturbations in the medium (dark shades) and without perturbations (light shades).

addresses directly the issue regarding the re-establishment of the connection on unfavorable conditions. Besides the RX-Improved Qi described in Section IV, we consider a heuristic for obtaining the best values of impedance, which maximize the charging current while respecting the maximum active power that the source can provide. It abstracts measurements and communication, generating a sample with 500 impedance values and then selecting the feasible ones that maximize the receiving current.

Fig. 6 shows the receiving voltage results for different simulated algorithms, considering 100 repetitions and 2 different cases. The first one admitted a 0.27% probability of link interruption, in a way similar to observations of real-world experiments, whereas the second one considered 0% of link interruption. The curve considering no perturbations and Resonant Ping method was omitted because it coincided with the curve of the case with link interruptions. The curve considering no perturbations and the regular Qi 1.0 was omitted for clarity purposes, since it is already shown in Fig. 5. Until about 20 mm apart, the system using the RX-Improved algorithm requires more power than the source can provide, and therefore, the "safe" value is applied instead of the result of the optimization algorithm. The "safe" value, for these experiments, is the internal impedance of the STEIN receiver (3.97 Ω equivalent resistance and 100 mF capacitance). In terms of transmission range, the algorithm is not prejudiced by this saturation condition, because the referred distance is not critical for the permanent loss of connection, even for regular Qi. Fig. 7 shows the receiving current readings, which are a constant factor away from the voltage curves since the equivalent load-impedance is kept constant throughout the experiments. Fig. 8, in turn, shows the transfer efficiency values considering only the case where the medium has no perturbations (0% link interruptions). The efficiency is calculated as the ratio between the power effectively dissipated by the load device and the power dissipated by all resistive components of the system, as shown in (11), where i_{RECT} is the received rectified current and R_L is the load resistance

$$\eta = \frac{R_L \cdot i_{\text{RECT}}^2}{R_T \cdot |i_T|^2 + R_R \cdot |i_R|^2}. \tag{11}$$

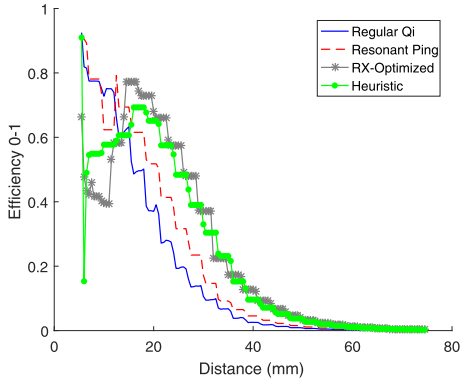

Fig. 8. Decay of the transfer efficiency in relation to the distance between the centroids of the coils (admitting no perturbations in the medium).

TABLE II
DESCRIPTIVE STATISTICS OF THE TRANSMITTING RANGES

	Mean	Median	Standard Deviation
Regular Qi 1.0	15.88	15.00	2.77
Resonant Ping	20.7	20.89	0.52
Optimal (estimation)	40.42	38.26	9.62
RX-Improved	44.89	49.18	11.7

We establish the transmission range as being the distance for which the voltage drops below 0.5 V. So, there is an independent sample of 100 ranges for each receiving strategy, whose descriptive statistics are shown in Table II. Notice that these statistics indicate that, at least under the conditions considered for the experiments, the transmitting range of the tested techniques follows the order *Rx-Improved>Heuristic>Resonant Ping>Regular Qi*. In order to better support this affirmation, we use multiple *Mann–Whitney* tests. The first one aims to testify that *RX-Improved>Heuristic*. It is structured as follows. Let r_1 be the transmitting range value for any execution of the RX-Improved Qi and r_2 the range for any execution of the heuristic. The null hypothesis claims that $P(r_2 \geq r_1) \geq 0.5$, whereas the alternative hypothesis claims $P(r_2 \geq r_1) < 0.5$. For the significance level $\alpha = 0.05$, the *p-value* achieves less

than 10^{-5} and, therefore, the null hypothesis is rejected. Indeed, analogous tests for the other consecutive pairs of samples of the order always reject the null hypotheses with *p-value* $< 10^{-5}$. Although not applicable from a practical point of view, the resonant ping method indicates that it is possible to mitigate the issue of permanent interruptions, since among the considered experiments these were not observed. Also, the RX-Improved Qi converges to the resonant state during the analog pings if the source is not saturated.

VI. Conclusion

Besides the fast decay of the magnetic flux between the coils with the distance, we identify the resilience as being a great issue for the enhancement of the range for Qi systems. We describe a method able to maximize the charging current by just acting over the impedance of the receiving part of a Qi-compliant system. In short, the transmitter must only respect the Qi Standard and, therefore, the algorithm does not require any additional information from it. The proposed method either reaches the maximum current or identifies that it is not currently able to do it. Experiments statistically prove that the transmitting range using RX-Improved Qi exceeds the range of the Regular Qi. Moreover, the algorithm improves the resilience of the communication link in such a way that not even a single permanent connection interruption was observed in all experiments.

Acknowledgment

The authors would also like to thank the research agencies CNPq and FAPEMIG.

References

[1] "Wireless power transmission market," 2014. [Online]. Available: https://www.ecmag.com/section/your-business/wireless-power-transmission-market-worth-170 4-billion-2020

[2] WPC, "Qi standard," 2008. [Online]. Available: https://www.wirelesspowerconsortium.com

[3] C. Raskind, "Qi wireless charging hit its stride in 2018 averaging over 1 million devices shipping daily," WPC, 2019. Accessed: Nov. 13, 2019. [Online]. Available: https://www.wirelesspowerconsortium.com/blog/

[4] Y. Peng, Z. Li, W. Zhang, and D. Qiao, "Prolonging sensor network lifetime through wireless charging," in *Proc. IEEE 31st Real-Time Syst. Symp.* IEEE, 2010, pp. 129–139.

[5] L. Xie, Y. Shi, Y. T. Hou, and H. D. Sherali, "Making sensor networks immortal: An energy-renewal approach with wireless power transfer," *IEEE/ACM Trans. Netw.*, vol. 20, no. 6, pp. 1748–1761, Dec. 2012.

[6] M. C. Domingo, "Magnetic induction for underwater wireless communication networks," *IEEE Trans. Antennas Propag.*, vol. 60, no. 6, pp. 2929–2939, Jun. 2012.

[7] J. Jadidian and D. Katabi, "Magnetic MIMO: How to charge your phone in your pocket," in *Proc. 20th Annu. Int. Conf. Mobile Comput. Netw.* New York, NY, USA: ACM, 2014, pp. 495–506.

[8] C. A. Floudas and P. M. Pardalos, "Quadratic fractional programming: Dinkelbach method, " in, *Encyclopedia of Optimization*. Berlin, Germany: Springer, 2001.

[9] A. L. A. Zuquim *et al.*, "Efficient power management in real-time embedded systems," in *Proc. IEEE Conf. Emerg. Technol. Factory Autom.* IEEE, 2003, pp. 496–505.

[10] N. A. Bhatti, A. A. Syed, and M. H. Alizai, "Sensors with lasers: Building a WSN power grid," in *Proc. 13th Int. Symp. Inf. Process. Sensor Netw*. IEEE Press, 2014, pp. 261–272.

[11] "Wireless power solutions" Powercast Corp, 2019. [Online]. Available: https://www.powercastco.com

[12] J. T. Hwang *et al.*, "21.8 An all-in-one (Qi, PMA and A4WP) 2.5 W fully integrated wireless battery charger IC for wearable applications," in *Proc. IEEE Int. Solid-State Circuits Conf*. IEEE, 2016, pp. 378–380.

[13] A. Berger, M. Agostinelli, C. Sandner, S. Vesti, and M. Huemer, "High efficient integrated power receiver for a QI compliant wireless power transfer system," in *Proc. IEEE Wireless Power Transfer Conf*. IEEE, 2016, pp. 1–4.

[14] H. Solar, M. Alonso, P. Bustamante, and C. Giers, "Design of a wireless power transfer receiver with an ad-hoc coil for the QI standard," in *Proc. Conf. Des. Circuits Integrated Syst*. IEEE, 2015, pp. 1–5.

[15] T. Duong and J.-W. Lee, "A dynamically adaptable impedance-matching system for midrange wireless power transfer with misalignment," *Energies*, vol. 8, no. 8, pp. 7593–7617, 2015.

[16] T.-D. Yeo, D. Kwon, S.-T. Khang, and J.-W. Yu, "Design of maximum efficiency tracking control scheme for closed-loop wireless power charging system employing series resonant tank," *IEEE Trans. Power Electron.*, vol. 32, no. 1, pp. 471–478, Jan. 2017.

[17] M. Fu, C. Ma, and X. Zhu, "A cascaded boost–buck converter for high-efficiency wireless power transfer systems," *IEEE Trans. Ind. Inform.*, vol. 10, no. 3, pp. 1972–1980, Aug. 2014.

[18] J. Kim and J. Jeong, "Range-adaptive wireless power transfer using multiloop and tunable matching techniques," *IEEE Trans. Ind. Electron.*, vol. 62, no. 10, pp. 6233–6241, Oct. 2015.

[19] R. Chen *et al.*, "Analysis and parameters optimization of a contactless IPT system for EV charger," in *Proc. 29th Annu. IEEE Appl. Power Electron. Conf. Expo*. IEEE, 2014, pp. 1654–1661.

[20] G. H. Golub and C. F. Van Loan, *Matrix Computations,* 4th ed. Baltimore, MD, USA: The Johns Hopkins Univ. Press, 2013.

[21] V. Liu, A. Parks, V. Talla, S. Gollakota, D. Wetherall, and J. R. Smith, "Ambient backscatter: Wireless communication out of thin air," in *Proc. ACM SIGCOMM*. New York, NY, USA: ACM, 2013, pp. 39–50.

[22] Y. Zeng, B. Clerckx, and R. Zhang, "Communications and signals design for wireless power transmission," *IEEE Trans. Commun.*, vol. 65, no. 5, pp. 2264–2290, May 2017.

[23] A. D. Sousa, L. F. M. Vieira, and M. A. M. Vieira, "Modeling, analysis and simulation of wireless power transfer," *Proc. 6th ACM Symp. Develop. Anal. Intell. Veh. Netw. Appl.*, 2017, pp. 143–150.

[24] A. D. Sousa, L. F. M. Vieira, M. A. M. Vieira, and J. A. M. Nacif, "Stein: Sistema de Transferência de Energia Para Internet Das Coisas," *Brazilian Symp. Comput. Syst. Eng.*, 2017.

Alexander D. de Sousa received the B.S. degree in 2017 from the Universidade Federal de Minas Gerais, Belo Horizonte, Brazil, where he is currently working toward the M.Sc. degree in computer science.

Luiz F. M. Vieira (Member, IEEE) received the undergraduate and M.S. degrees with the Universidade Federal de Minas Gerais (UFMG), Belo Horizonte, Brazil, in 2002 and 2004, respectively, and the Ph.D. degree in computer science from the University of California Los Angeles, Los Angeles, CA, USA, in 2009.

He is currently an Associate Professor with the Computer Science Department, UFMG. His research interests include computer networking, wireless networks, and wireless power transfer. Dr. Vieira was awarded a productivity in research scholarship from CNPq.

Marcos A. M. Vieira (Member, IEEE) received the undergraduate and M.S. degrees from Universidade Federal de Minas Gerais (UFMG), Belo Horizonte, Brazil, in 2002 and 2004, respectively, and the Ph.D. degrees in computer science from the University of Southern California, Los Angeles, CA, USA, in 2010.

He is currently an Associate Professor with the Computer Science Department, UFMG. His research interests include computer networking, wireless networks, and wireless power transfer.

Dr. Vieira was awarded a productivity in research scholarship from CNPq.